Journal of Materials Chemistry C

Accepted Manuscript

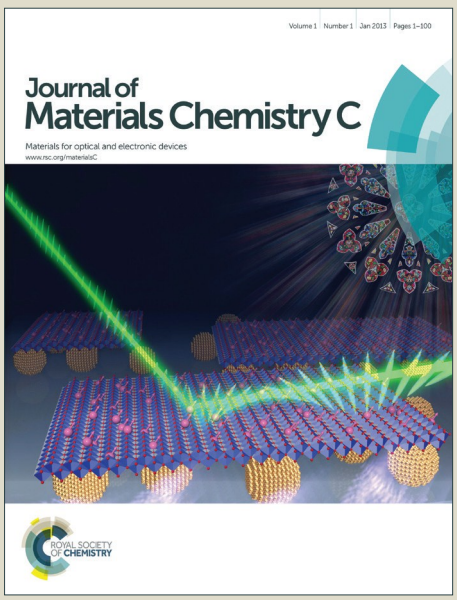

ROYAL SOCIETY OF CHEMISTRY

www.rsc.org/materialsC

Heterovalent substitution in anionic and cationic positions of PbS thin-films grown by SILAR method vis-à-vis Fermi energy measured through scanning tunneling spectroscopy

Hrishikesh Bhunia, Biswajit Kundu, Soumyo Chatterjee and Amlan J. Pal*

Department of Solid State Physics, Indian Association for the Cultivation of Science, Jadavpur, Kolkata 700032, India

E-mail: sspajp@iacs.res.in.

Keywords: Heterovalent substitution in IV-VI semiconductor; altervalent cation substitution and aliovalent anion substitution; mono- and tri-valent elements as dopants; introduction of free carriers; scanning tunneling spectroscopy; shift in Fermi energy; SILAR technique.

ABSTRACT. We report growth and characterization of doped-PbS thin-films deposited by a successive ionic layer adsorption and reaction (SILAR) method. Altervalent cation and aliovalent anion substitution through ions of mono- and trivalent elements as dopants have been achieved in the compound semiconductor. Here the heterovalent elements introduced free carriers in the semiconductors, the nature of which depended on its valency and the ions it substituted in the compound. Effect of such dopants on the Fermi energy of PbS has been followed by scanning tunneling spectroscopy (STS) that has correspondence to density of states (DOS) of a semiconductor. By locating conduction and valence band-edges of the pristine and different doped-semiconductors, the STS studies provided a direct evidence of a shift in Fermi energy upon heterovalent cationic and anionic substitution in compound semiconductors.

1. Introduction

Semiconducting metal chalcogenides are of immense importance due to their applications in a range of electronic and optoelectronic devices.[1] Some of the chalcogenides have an ultralow thermal conductivity that is a prerequisite for their use as thermoelectric power generation materials.[2-5] Some of them have a suitable band gap to match the Shockley–Queisser limit of solar conversion efficiency.[6-8] Material-dependent band gap of such chalcogenides has also enabled formation of heterojunctions having a type-II or staggered band gap at the interface that is instrumental in separation of charge carriers in solar cells.[6-8] As both thermoelectric and photovoltaic materials, carrier concentration or more-specifically the nature of semiconductor is indeed an extremely important parameter.

In order to tune the carrier concentration, introduction of dopants is a preferred route over selecting a metal or a chalcogen in forming a chalcogenide, since the use of a different element would alter also the band gap.[4,5,9,10] As opposed to an isovalent cation or anion substitution, heterovalent ones, on the other hand, introduce carriers and hence affects conductivity and other electrical properties of the semiconductor keeping the band gap mostly unaltered. While an altervalent cation substitution is somewhat common in II-VI and IV-VI compound semiconductors and its higher-fold derivatives, such as $I-III-VI_2$, $I_2-II-IV-VI_4$, and so forth in their quantum-dot or thin-film equivalent forms,[4,10-13] researchers have initiated to work on aliovalent anion substitution[5,14-18] to open newer routes to tune carrier concentration and hence Fermi energy of the semiconductors. Aliovalent anion substitution affected (lowered) also the band gap in some materials including oxides.[18]

A range of elements can be used as a substituent in compound semiconductors yielding different effects. For example, in binary semiconductors based on a divalent metal, a monovalent cation substitution would introduce one extra hole thereby shifting the Fermi energy towards the valence band (VB). Similarly, a trivalent metal would bring a free-

electron leading to formation of an *n*-type semiconductor. Substitution at the anionic sites would have an opposite effect. While each halide substitution at the chalcogen sublattice would introduce an electron shifting the Fermi energy towards the conduction band (CB), introduction of trivalent anions would on the other hand lead to formation of a *p*-type semiconductor.

It is therefore imperative to locate the Fermi energy upon substitution of different altervalent and aliovalent elements at the cationic and anionic sites, respectively. In this direction, scanning tunneling spectroscopy (STS) studies can be truly appropriate. STS studies are known to provide differential conductance (d*I*/d*V*) spectrum that has correspondence to the density of states (DOS) of a semiconductor or complex nanostructures.[9,19-23] From the d*I*/d*V* spectra, CB and VB edges could be located in the form of peaks in either sides of the voltage-axis; here the band-edges are located with respect to the semiconductor's Fermi energy which is considered to be aligned at 0 V. In other words, STS of heterovalent-doped binary semiconductors would allow us to follow the shift in Fermi energy upon substitution at the anionic and cationic sites. In this work, we have formed ultrathin-films of lead sulfide (PbS) through a successive ionic layer adsorption and reaction (SILAR) method. As such, this film deposition method, which is a room temperature one, offers a range of advantages including film-formation on a variety of substrates for flexible (opto)electronics.[24] Moreover, dopants can also be introduced to tailor the semiconductor for device applications. During the film formation, we introduced mono- and trivalent elements at the cationic and anionic sites. We then studied the *p*-and *n*-type nature of the semiconductors from STS of PbS and different doped-PbS films by locating their Fermi energy and band-edges.

2. Experimental section

2.1 Materials

Lead(II) acetate trihydrate, $Pb(CH_3COO)_2 \cdot 3H_2O$, sodium sulfide hydrate, $Na_2S \cdot xH_2O$, silver nitrate ($AgNO_3$), tetrabutylammonium halides, $[CH_3(CH_2)_3]_4NX$ (X = Cl, Br, I) and triphenylphosphine, $(C_6H_5)_3P$ were purchased from Merck Chemicals. Bismuth(III) acetate, $Bi(CH_3COO)_3$ was purchased from Alfa Aesar. All the compounds were used without any further purification.

2.2 Growth of PbS thin films by SILAR method

Thin films of PbS were grown on *n*-type Si<111> and quartz substrates following a reported procedure[25,26] in a multi-vessel dip-coater. The substrates were first cleaned via a usual protocol. Lead acetate (0.02 M) and sodium sulfide (0.02 M) in 20 mL methanol each were used as cationic and anionic precursor solutions, respectively. To grow the films, the substrates were first dipped in the cationic bath for adsorption of Pb^{2+} ions. After immersing the substrates in methanol to remove loosely bound ions, they were then dipped in the anionic precursor solution for reaction to occur that formed the metal chalcogen (PbS). Finally the substrates were immersed in another methanol bath for a thorough rinsing. While dipping and lifting of the substrates occurred at a speed of 400 mm/min, they were kept in the precursors (and in methanol) for 1 min each; additionally, the substrates were air-dried after rinsing in methanol. These four steps completed one SILAR cycle, which was repeated for a desired number of times to achieve a particular thickness of the semiconductor.

2.3 Doping in PbS thin-films

We intended to introduce mono- and trivalent cationic and anionic substitutes. While silver and bismuth were considered for replacement of Pb^{2+} ions, a range of halides and phosphides were chosen for the chalcogen sites.

- *Monovalent cation substitution.* A stoichiometric amount of silver nitrate ($AgNO_3$) in deionized water that acted as a source of silver ions was added to the cationic precursor solution in ethanol. Volume ratio of ethanol and water was 1:1. The anionic precursor and dipping protocol remained the same. We have also varied the silver content in doped-PbS thin films so that atomic% of silver with respect to lead became 1-6 % in a step of 1.
- *Trivalent cation substitution.* To introduce bismuth ions in place of lead, $Bi(CH_3COO)_3$ powder was added to the cationic precursor solution. pH of the methanol solution was adjusted to 4.2 by adding glacial acetic acid. Here too, the anionic precursor and dipping protocol remained the same; bismuth content in doped-PbS thin films was 3 atomic% with respect to lead.
- *Monovalent anion substitution.* We introduced a range of halides (chloride, bromide, and iodide) in place of sulfide to form aliovalent anion-substituted PbS thin-films. To achieve chloride substitution, $[CH_3(CH_2)_3]_4NCl$ was added to the anionic precursor solution. For bromide and iodide substitution, equivalent salts were used in the sodium sulfide solution. The halide content in doped-PbS thin films was 3 atomic% with respect to sulfide. In this case, the cationic precursor and dipping protocol remained the same.
- *Trivalent anion substitution.* To introduce phosphide ions in place of sulfide, $(C_6H_5)_3P$ was added to the methanol solution of Na_2S. The phosphide content that we intended to achieve in PbS thin-films was 3 atomic% with respect to sulfide.

2.4 Characterization of PbS and doped-PbS thin-films

Optical absorption spectroscopy, X-ray diffraction (XRD) analysis, and X-ray photoelectron spectroscopy (XPS) of the materials were recorded with a UV-Vis-NIR Spectrophotometer (Cary 5000, Agilent Technologies), Bruker D8 Advanced X−ray Powder Diffractometer (Cu K_α radiation, $\lambda = 1.54$ Å), and an XPS instrument (Omicron: serial no. 0571), respectively. In addition, atomic force microscopy (AFM) and scanning electron microscopy (SEM) images of their ultrathin SILAR films were recorded with Nanosurf Easyscan2 AFM and JEOL JSM 6700F field emission SEM, respectively. Scanning tunneling spectroscopy (STS) of a monolayer of as-formed PbS and different doped-PbS were recorded in a scanning tunneling microscope (STM, Easyscan2 of Nanosurf AG) in an ambient condition. While the semiconductors were deposited on highly-doped silicon wafers (*n*-type, As-dopant) having a resistivity of 3-10 mΩ·cm, bias was applied to the STM's Pt/Ir (80%:20%) tip which was formed through cutting a wire of 0.25 mm diameter.

To study charge separation process in the semiconductors and in junctions between two semiconductors, thin-films were formed on indium tin oxide (ITO) coated glass substrates. As top electrodes, aluminum strips were thermally evaporated on the active layer to form sandwiched-structures, current-voltage ($I-V$) characteristics of which were recorded with a Keithley 2636 Electrometer using LabTracer software. A 150 W Newport-Stratfort Solar Simulator model 76500, attached with an AM1.5 filter, acted as a source for illumination.

3. Results and discussion

3.1 Characterization of the films

To monitor growth of films formed through SILAR method, we recorded optical absorption spectroscopy of the films after deposition of each layer. Such spectra of PbS and doped-PbS for 10-layered SILAR films are shown in Fig. 1(a). The spectra that extend till the near-IR region match that of PbS films formed through SILAR and other methods.[27] A variation in absorbance for different films may have arisen due to a difference in pH of the cationic/anionic solutions upon addition of salts of the dopants. Growth of the films has been presented as a plot of absorbance versus number of layers for PbS and different doped-PbS (Fig. 1b). The absorbance in general grew linearly evidencing the success of the SILAR method. To infer if the dopants influenced optical gap of the semiconductor, we converted the absorption spectra to Tauc plots of the materials (Fig. 1c). The optical gap, as obtained from a rough estimate of the linear region, appears to have ranged between 1.18 and 1.25 eV; for aliovalent anion substitutions, the band gap was slightly lower as compared to that of the pristine or the metal-substituted semiconductors. The results however inferred that the heterovalent dopants did not influence the optical gap of the semiconductors in a large way. The thickness of the films that were required to make Tauc plots were measured by recording surface profile of an intentional scratch on each the films with AFM (Fig. 1d and Fig. S1, ESI†). The surface profile of the AFM images moreover show the uniformity of the deposited films through SILAR method.

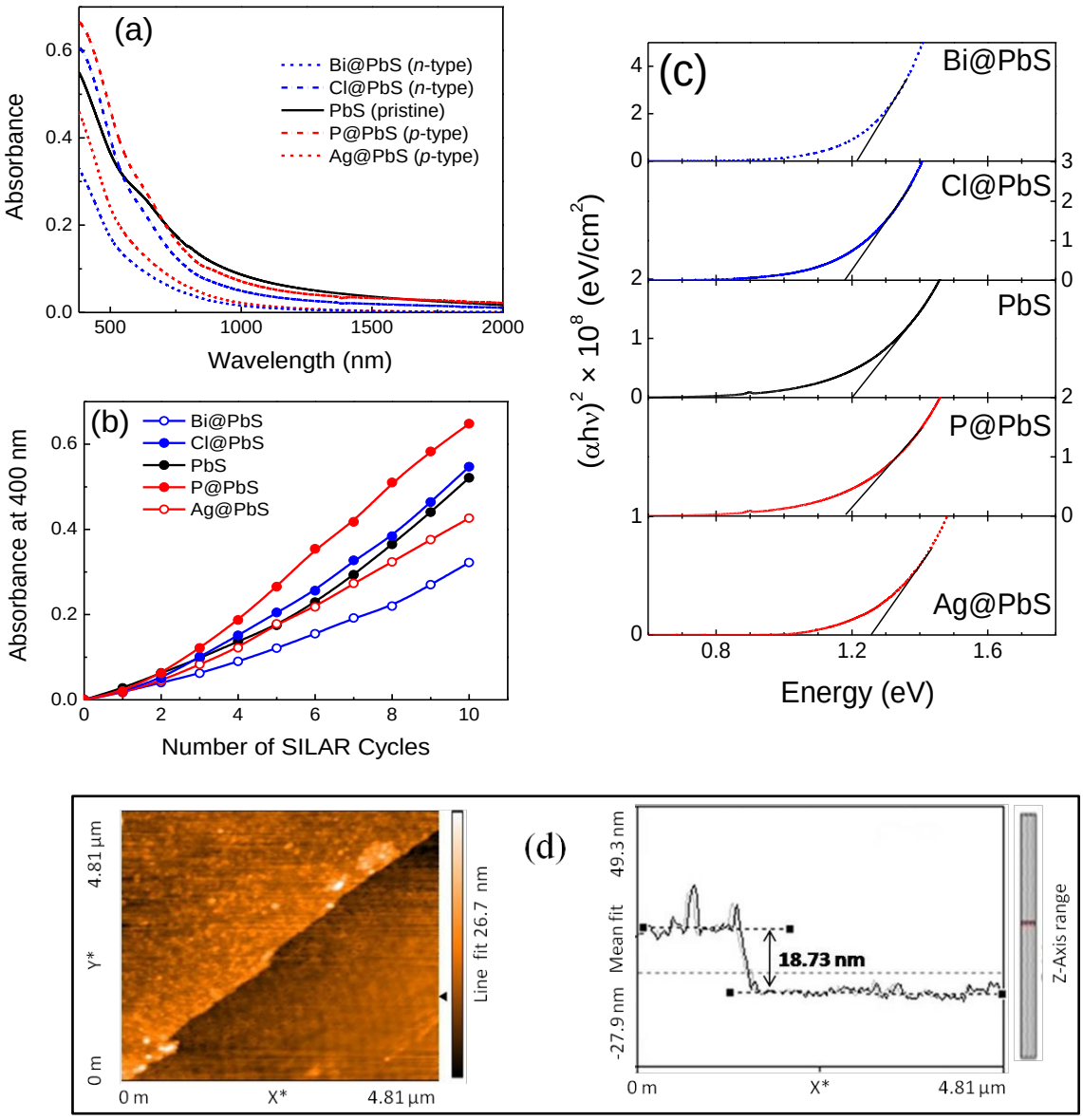

Fig. 1 (a) Optical absorption spectra of PbS and different doped-PbS films as stated in the legends having 10 SILAR layers each. (b) Absorbance at 400 nm versus number of layers of the materials. (c) Tauc plots to determine optical band gap of the semiconductors (as shown by straight lines). (d) AFM image of a scratched 10-layer PbS SILAR film along with the depth profile of the scratch.

In order to ensure formation of PbS crystalline thin-films and conclude on dopants' position in the lattice, the pristine and doped-PbS materials were characterized following usual processes. In Fig. 2, we present XRD patterns of the thin-films. Diffraction patterns of

PbS are in concurrence with Joint Committee on Powder Diffraction Standards (JCPDS) file #05-0592 inferring its formation and presence of a single phase. For the doped crystals, the peaks in the pattern did not show any noticeable shift in diffraction angles; neither any new peak appeared in such spectra. The dopants hence did not form any new phases in the crystalline thin-films. Invariance of XRD patterns upon introduction of dopants moreover inferred that the cationic and anionic dopant-ions substituted the corresponding sites, that is, either Pb^{2+} or S^{2-} sites, respectively, in forming doped-PbS crystalline thin-films. Substitution of mono- or tri-valent ions (Ag^{+}, Bi^{3+}, Cl^{-}, P^{3-}) at the lead or sulfide sites is expected since the salts of the dopants that were used were soluble in methanol; with PbS being insoluble in methanol, the salts of dopants (such as silver nitrate, tetrabutylammonium halides, and so forth) if formed on the substrate would have re-dissolved leaving only the doped-PbS on a substrate.

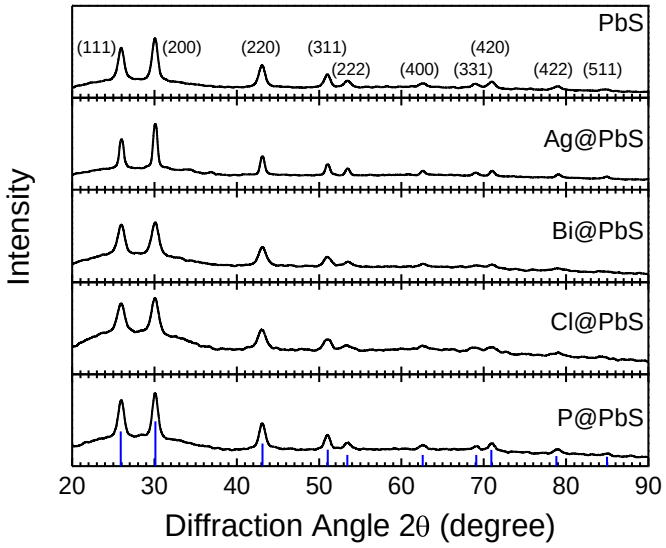

Fig. 2 XRD patterns of pristine and different doped-PbS thin-films. Sticks placed at the abscissa represent the patterns as per the JCPDS file of cubic (cF8) PbS.

To know if the content of dopant that we aimed for during the SILAR process (3.0 atomic%) was truly transferred to the doped-PbS films, we carried out EDX analyses of the materials. While the analysis of PbS evidenced presence of lead and sulfur having a proper

stoichiometric ratio, presence of dopants could be envisaged in the analyses of doped materials. The results have been summed up in Table 1 in the form of weight% and atomic% of the elements in PbS and doped-PbS thin-films. We could infer that the content of dopants in doped-PbS ranged between 3.4-7.7 atomic% with respect to the cation/anion. The range matched reasonably well with that was aimed through addition dopants in the precursor solutions. A dopant-dependent adsorption may have occurred in the thin-films due to a variation of pH upon addition of salts in the cationic or anionic precursor solutions.

Table 1 EDX analysis of PbS and doped-PbS thin-films showing the weight percents and atomic percents of the elements present in the materials along with concentration of cationic and anionic dopants with respect to lead ions or sulfides, respectively.

Material	Weight% of Elements			Atomic% of Elements			Dopant concentration achieved (atomic%)
	Pb	S	Dopant	Pb	S	Dopant	
PbS	87.8	12.1	-	52.89	47.11	-	-
Ag@PbS	87.7	9.33	2.98	57.05	39.22	3.72	6.52
Bi@PbS	83.8	13.4	2.87	48.37	49.98	1.64	3.39
Cl@PbS	88.2	11.1	0.71	53.85	43.62	2.53	5.80
P@PbS	85.7	13.3	0.99	48.07	48.21	3.71	7.70

To gather further information on the valence state of the elements, we carried out XPS analysis of PbS and doped-PbS thin-films. Fig. 3 represents the obtained results for PbS that were corrected considering the peak of C1s to be at 284.5 eV. The peaks of PbS matched the reported binding energies corresponding to Pb4f and Pb4d electrons of Pb^{2+} and S2p and S2s electrons of S^{2-} inferring formation of PbS in the thin-films.[16] We further recorded high-resolution spectra in energies closer to the peaks corresponding to Pb4f and Pb4d electrons (Figs. 3b and 3c). Such spectra show that the Pb4f peak resolved into 139.0 and 143.9 eV

representing $4f_{7/2}$ and $4f_{5/2}$, respectively. Similarly, the Pb4d resolved at 414.4 and 436.5 eV that represented binding energies of $4d_{5/2}$ and $4d_{3/2}$ states, respectively. The binding energies corresponding to S2p and S2s electrons of S^{2-} appeared at 163.6 and 226.0 eV, respectively. In the XPS spectra of doped-PbS, binding energies of dopants' core-electrons appeared in addition (Fig. S2, ESI†) inferring their presence in the semiconductors.

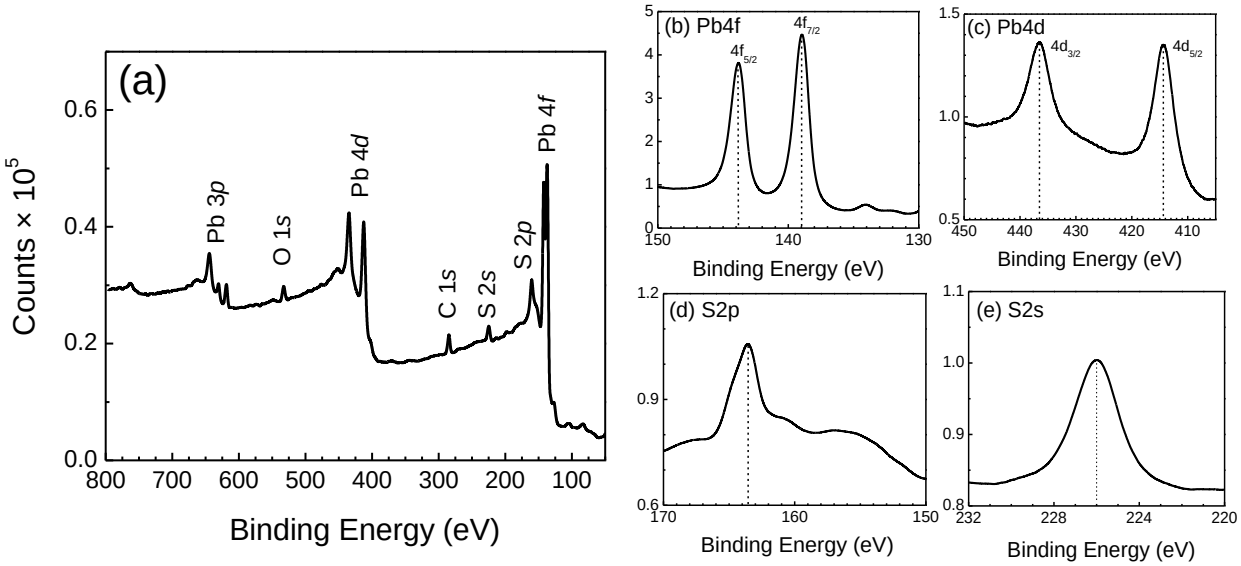

Fig. 3 (a) Full-range XPS spectrum of pristine PbS. High-resolution spectra of the material resolving binding energies of Pb4f, Pb4d, S2p, and S2s electrons are shown in (b) through (e), in sequence.

In order to study the morphology of the PbS and doped-PbS thin-films formed by SILAR method, we have recorded SEM images of such films. Fig. S3 (ESI†) displays such an image of a PbS thin-film. The image evidenced that the SILAR films were uniform in nature without any pin-holes or cracks representing superior quality of the films formed through this method.

3.2. Scanning tunneling spectroscopy

In order to locate the Fermi energy of PbS and different doped-PbS semiconductors, we recorded tunneling current at many different points on each of the ultrathin-films. Measurements were carried out after disabling the feedback-loop of the STM. The peaks in the dI/dV versus voltage plots, which have correspondence to the density of states (DOS) of a semiconductor, provided the position of CB and VB edges. Since the voltage was applied to the tip with respect to the substrate, the peaks in the negative voltage region of DOS spectra implied electron-injection to the semiconductor and hence denoted CB of a semiconductor. Similarly, the peaks at positive voltages, at which electrons could be withdrawn from a semiconductor, provided the location of the VB. For each of the semiconductors, since we recorded tunneling current at many different points, we show a typical DOS spectrum in Fig. 4(a). The spectrum depicts characteristics of intrinsic PbS in thin-film form. The plot brings out CB and VB edges as peaks in the negative and positive tip-biases, respectively, with respect to the Fermi energy which is considered to be aligned at 0 V. The results obtained from around 100 points on the thin-film have been summed up as a histogram of CB and VB energies (Fig. 4b). Such a plot shows that the band edges were 0.66 and 0.58 eV apart from the Fermi energy, respectively, for the undoped PbS thin-films. The histogram moreover evidenced that the Fermi energy was closer to the VB edge inferring *p*-type nature of the semiconductor in pristine thin-films.

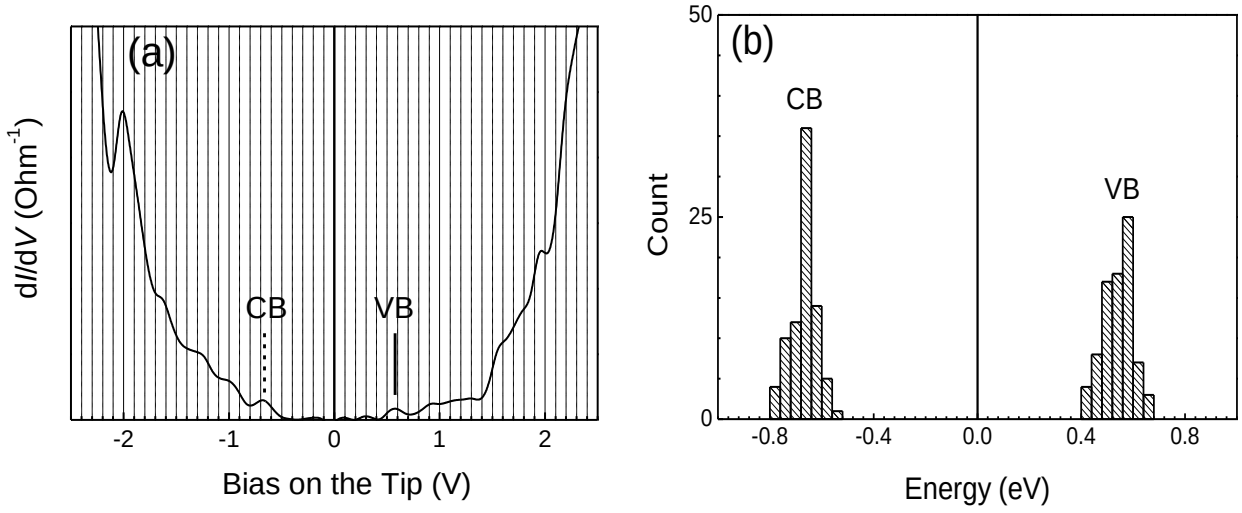

Fig. 4 (a) Numerical derivative of $I-V$ characteristics versus tip-voltage plots of pristine PbS ultrathin-films. The CB and VB edges of the semiconductor are marked with vertical broken and straight lines at the negative and the positive voltage, respectively. (b) Histogram of CB and VB edges as obtained from DOS measured at about 100 spots on the thin-film.

To obtain the CB and VB energies of the doped-PbS semiconductors, we similarly recorded tunneling current on each of the ultrathin films. Here also, measurements were carried at many different points. In Figs. 5 and 6, we show typical dI/dV versus voltage plots and histograms of CB and VB energies for the Ag, Bi, Cl, and P-doped PbS semiconductors, respectively. With 0 V being aligned to Fermi energy in each of the cases, the plots show that the Fermi energy shifted within the gap upon introduction of dopants. When we compare the results with respect to pristine-PbS, the Fermi energy of Ag@PbS shifted towards the VB since a monovalent cation (Ag^{+}) introduced one extra hole in the system; the Ag@PbS hence became a *p*-type semiconductor. The Bi@PbS, on the other hand acted as an *n*-type semiconductor (even with respect to undoped-PbS); here the Fermi energy shifted towards the CB since each Bi^{3+} brought a free-electron in the lattice. For the aliovalent anion substitution, the halides converted the semiconductor to be an *n*-type due to introduction of electrons; the Fermi energy of P@PbS shifted towards the VB edge evidencing *p*-type nature of the doped semiconductor.

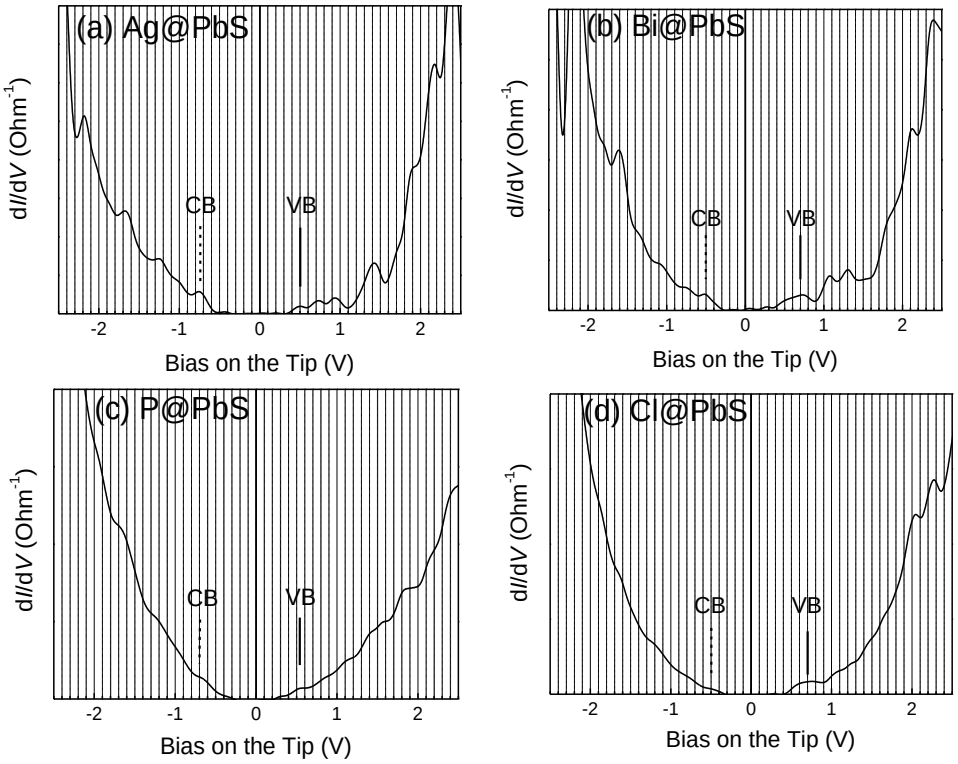

Fig. 5 Numerical derivative of $I-V$ characteristics versus tip-voltage plots for different doped-PbS ultrathin-films. The CB and VB edges of the doped-semiconductor are marked with vertical broken and straight lines at the negative and the positive voltages, respectively.

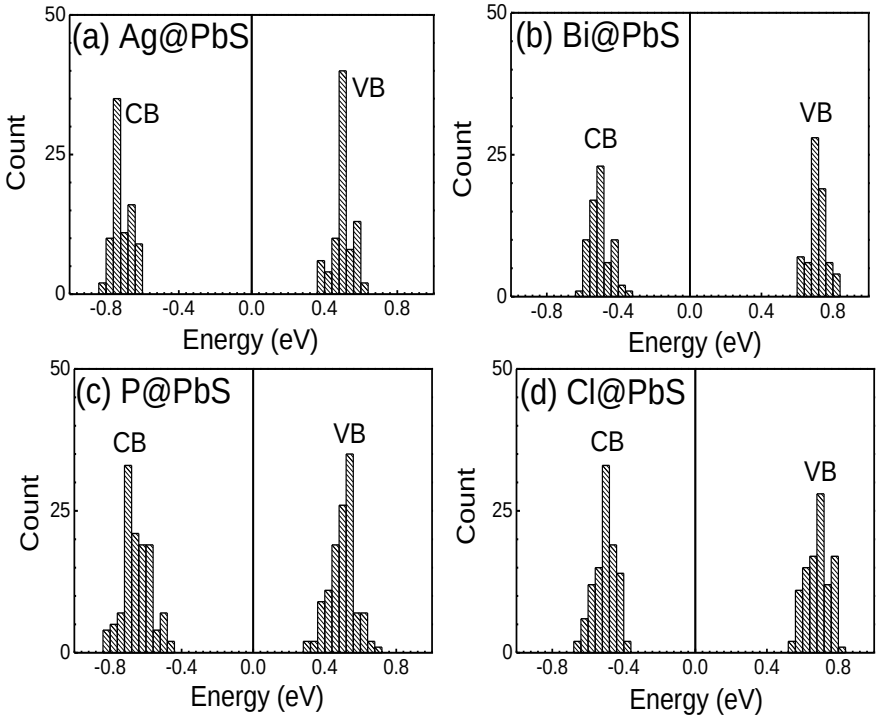

Fig. 6 Histogram of CB and VB edges of different doped-PbS as obtained from DOS measured at about 100 spots on each thin-film.

3.3. Band diagram and transport gap

The results have been summed up as band-diagrams of the semiconductors (Fig 7). With the ordinate of plot being energy with respect to the Fermi level, the diagram clearly shows that Fermi energy shifted towards the VB in Ag- and P-substituted PbS. For the Bi- and Cl-doped cases, the Fermi energy shifted towards the CB. The results hence infer that a binary semiconductor can be made *p*- or *n*-type by introducing suitable heterovalent cation and anion substitutions during the film formation process.

It may be added that we also studied the effect of dopant-concentration on the shift of Fermi energy. For such studies, we considered silver as the substituent, whose concentration in the cationic precursor solution with respect to lead ions was varied from 1 to 6 atomic%. From the DOS spectra, we observed that the Fermi energy shifted progressively towards the VB edge upon an increase in silver-concentration in Ag@PbS thin-films (Fig. S4, ESI†). The results support the thesis that each silver ion while substituting a lead one introduces one extra hole in the system. We also considered different halides as aliovalent anion dopants. When such results were compared, the shift in Fermi energy towards the CB was the highest for chloride (Fig. S5, ESI†). With iodide yielding a least shift in the Fermi energy, the effect of bromide on the shift was intermediate implying that electronegativity of the dopants must have influenced their substitution process and thereby the introduction of free-electrons in the doped semiconductors.

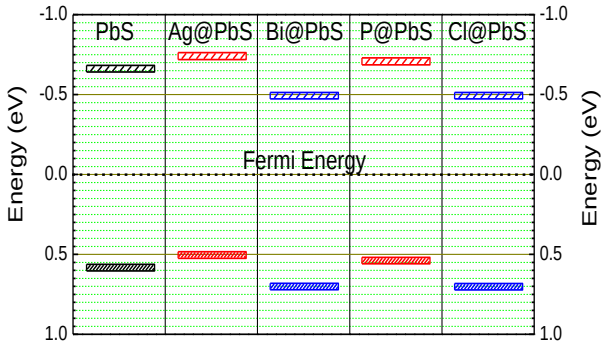

Fig. 7 Schematic band diagram of PbS and different doped-PbS thin-films formed through SILAR technique. The dashed line represents each semiconductor's Fermi energy, which was aligned to 0 V.

Transport gap, which is the difference between the CB and VB edges as obtained from the DOS spectra and corresponding histogram, did not vary by a significant amount upon heterovalent substitution. This is expected since the dopants are known to affect the Fermi energy of the semiconductor in a usual manner. Histogram of transport gap, as obtained from the difference in CB and VB energies of PbS and different doped-PbS are shown in Fig. 8. The plots show that the transport gap and its distribution over the measurements did not vary upon doping; they neither depended on the type of the substituent (cationic or anionic) or their effects in forming *p*- or *n*-type semiconductors. A comparison of optical band gap (as obtained from Tauc plots) and transport gap of PbS and different doped-PbS semiconductors are presented in Table 2, although determination of optical gaps is involved with a certain level of inaccuracy. The data show that the neither of them expectedly varied upon introduction of dopants. Since the measurement of transport gaps has a higher degree of precision, the extent of variation (in the transport gap) was also smaller than that of the optical gap. The results hence infer that suitable heterovalent substituent of cationic or anionic nature can be introduced in a binary semiconductor during the layer-by-layer growth process to obtain a desirably-doped semiconductor.

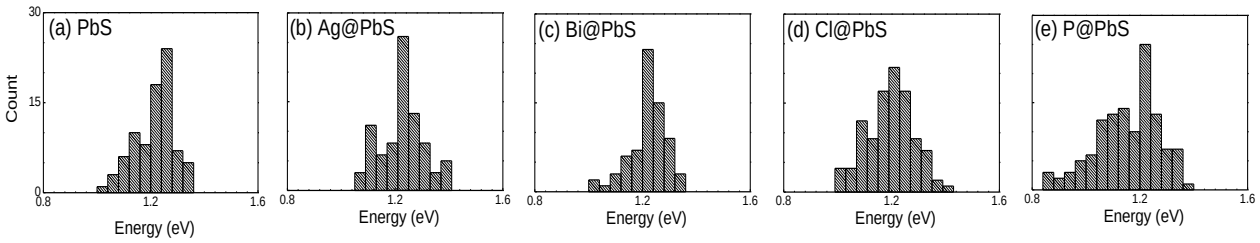

Fig. 8 Histogram of transport gap of PbS and different doped-PbS semiconductors as obtained from DOS measured at about 100 spots on each thin-film.

Table 2 Optical gap and transport gap of PbS and doped-PbS thin-films

Material	Optical gap from Tauc plots (eV)	Transport gap from DOS (eV)
PbS	1.20	1.26
Ag@PbS	1.26	1.23
Bi@PbS	1.21	1.22
Cl@PbS	1.18	1.21
P@PbS	1.18	1.22

The shift in Fermi energy upon introduction of dopants can also be evidenced by studying charge separation process when the semiconductors were sandwiched between two electrodes. To do so, we characterized a bilayer *pn*-junction under illumination and compared the characteristics with that of Schottky diodes based on the components of the junction. In effect, we formed sandwiched structures of *p*-type Ag@PbS, *n*-type Cl@PbS, and of Ag@PbS/Cl@PbS homojunction between ITO and aluminum electrodes. Total thickness of the active layer in Schottky diodes and in the *pn*-junction was the same (100 nm) to achieve invariant photoabsorption. Dark characteristics of the three devices were rectifying in nature suggesting that photovoltaic response can be observed in such devices under illumination. In Fig 9, we present $I-V$ characteristics of the sandwiched structures under illumination. Photovoltaic parameters of the devices have been summed up in Table 3. The results show

superior photovoltaic parameters in the *pn*-homojunction as compared to those from the Schottky diodes inferring an efficient charge separation process in the former device. In the Ag@PbS/Cl@PbS *pn*-junction, a type-II band-alignment must have formed due to *p*-nature of Ag@PbS and *n*-type nature of Cl@PbS expediting charge separation at the interface. The results hence support the observation of shift in Fermi energy upon introduction of dopants in PbS.

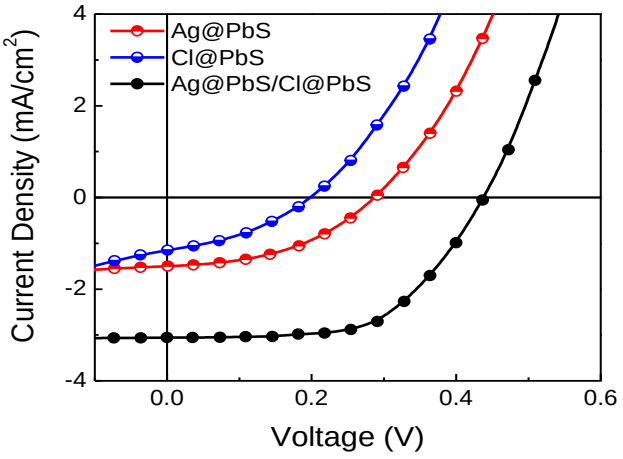

Fig. 9 Current-voltage characteristics of the active layers (as stated in the legends) sandwiched between ITO and aluminum electrodes under 1 Sun illumination condition.

Table 3 Photovoltaic parameters of the devices under 1 Sun.

Active layer	Short-circuit Current (mA/cm^2)	Open-Circuit Voltage (V)	Fill-Factor (%)	Energy Conversion Efficiency (%)
Ag@PbS	1.50	0.29	44	0.19
Cl@PbS	1.15	0.19	38	0.08
Ag@PbS/Cl@PbS	3.05	0.43	59	0.78

4. Conclusions

In conclusion, we introduced heterovalent dopants during formation of PbS thin-films through SILAR technique. While Ag and Bi-ions were incorporated as altervalent cationic substitution, a range of halides and phosphides acted as aliovalent anionic dopants. From STS

of the semiconductors in order to locate their band-edges with respect to its Fermi energy, we observed that the heterovalent-substitution introduced free-carriers in PbS and thereby altered the type of the semiconductor. The nature of free-carriers depended on the valency and nature of dopants. From the STS studies, we observed that a monovalent cation (Ag^{+}) introduced one extra hole in the system and thereby shifted the Fermi energy of Ag@PbS towards the VB edge. In Bi@PbS, each Bi^{3+} brought a free-electron in the lattice shifting the Fermi energy towards the CB. For aliovalent anion substitution, halides converted the semiconductor to be *n*-type in nature due to introduction of electrons. The Fermi energy of P@PbS shifted towards the VB edge evidencing *p*-type nature of the doped semiconductor. STS studies presented in this work provided a direct evidence of a shift in Fermi energy upon heterovalent cationic and anionic substitution in a compound semiconductor.

Acknowledgements

HB acknowledges CSIR Fellowship No. 09/080(0958)/2014-EMR-I (Roll No. 521931). SC acknowledges DST INSPIRE Fellowship (IF 140158). The authors acknowledge financial assistance from Nano Mission (DST) projects.

† **Electronic supplementary information (ESI) available:** The characterization section including Atomic Force Microscopy images, XPS analysis, SEM images, and plots of band diagram. See DOI: 10.1039/x0xx00000x

References

1 I. Chung, M. G. Kanatzidis, *Chem. Mater.*, 2014, **26**, 849-869.

2 J. P. Heremans, V. Jovovic, E. S. Toberer, A. Saramat, K. Kurosaki, A. Charoenphakdee, S. Yamanaka, G. J. Snyder, *Science*, 2008, **321**, 554-557.

3 S. Johnsen, J. Q. He, J. Androulakis, V. P. Dravid, I. Todorov, D. Y. Chung, M. G. Kanatzidis, *J. Am. Chem. Soc.*, 2011, **133**, 3460-3470.

4 T. C. Harman, M. P. Walsh, B. E. Laforge, G. W. Turner, *J. Electron. Mater.*, 2005, **34**, L19-L22.

5 S. N. Guin, V. Srihari, K. Biswas, *J. Mater. Chem. A*, 2015, **3**, 648-655.

6 Y. Wang, H. Gong, B. H. Fan, G. X. Hu, *J. Phys. Chem. C*, 2010, **114**, 3256-3259.

7 A. K. Rath, M. Bernechea, L. Martinez, G. Konstantatos, *Adv. Mater.*, 2011, **23**, 3712-3717.

8 Y. Firdaus, E. Vandenplas, Y. Justo, R. Gehlhaar, D. Cheyns, Z. Hens, M. Van der Auweraer, *J. Appl. Phys.*, 2014, **116**, 094305.

9 D. Mocatta, G. Cohen, J. Schattner, O. Millo, E. Rabani, U. Banin, *Science*, 2011, **332**, 77-81.

10 A. Sahu, M. S. Kang, A. Kompch, C. Notthoff, A. W. Wills, D. Deng, M. Winterer, C. D. Frisbie, D. J. Norris, *Nano Lett.*, 2012, **12**, 2587-2594.

11 H. Liu, D. Zhitomirsky, S. Hoogland, J. Tang, I. J. Kramer, Z. J. Ning, E. H. Sargent, *Appl. Phys. Lett.*, 2012, **101**, 151112.

12 A. Stavrinadis, A. K. Rath, F. P. G. de Arquer, S. L. Diedenhofen, C. Magen, L. Martinez, D. So, G. Konstantatos, *Nat. Commun.*, 2013, **4**, 2981.

13 N. N. Zhang, X. P. Zou, Y. Y. Gao, *Int. J. Photoenergy*, 2015, 326850.

14 K. Ohkawa, T. Mitsuyu, O. Yamazaki, *J. Appl. Phys.*, 1987, **62**, 3216-3221.

15 L. M. Moreau, D. H. Ha, C. R. Bealing, H. T. Zhang, R. G. Hennig, R. D. Robinson, *Nano Lett.*, 2012, **12**, 4530-4539.

16 D. Zhitomirsky, M. Furukawa, J. Tang, P. Stadler, S. Hoogland, O. Voznyy, H. Liu, E. H. Sargent, *Adv. Mater.*, 2012, **24**, 6181-6185.

17 S. Kouser, S. R. Lingampalli, P. Chithaiah, A. Roy, S. Saha, U. V. Waghmare, C. N. R. Rao, *Angew. Chem.-Int. Edit.*, 2015, **54**, 8149-8153.

18 C. N. R. Rao, *J. Phys. Chem. Lett.*, 2015, **6**, 3303-3308.

19 D. Katz, T. Wizansky, O. Millo, E. Rothenberg, T. Mokari, U. Banin, *Phys. Rev. Lett.*, 2002, **89**, 086801.

20 K. Overgaag, P. Liljeroth, B. Grandidier, D. Vanmaekelbergh, *ACS Nano*, 2008, **2**, 600-606.

21 D. Steiner, D. Dorfs, U. Banin, F. Della Sala, L. Manna, O. Millo, *Nano Lett.*, 2008, **8**, 2954-2958.

22 A. Bera, S. Dey, A. J. Pal, *Nano Lett.*, 2014, **14**, 2000-2005.

23 S. U. Nanayakkara, J. van de Lagemaat, J. M. Luther, *Chem. Rev.*, 2015, **115**, 8157-8181.

24 M. Q. Fang, H. M. Jia, W. W. He, Y. Lei, L. Z. Zhang, Z. Zheng, *Phys. Chem. Chem. Phys.*, 2015, **17**, 13531-13538.

25 H. M. Pathan, C. D. Lokhande, *Bull. Mat. Sci.*, 2004, **27**, 85-111.

26 H. Lee, H. C. Leventis, S. J. Moon, P. Chen, S. Ito, S. A. Haque, T. Torres, F. Nuesch, T. Geiger, S. M. Zakeeruddin, M. Gratzel, M. K. Nazeeruddin, *Adv. Funct. Mater.*, 2009, **19**, 2735-2742.

27 V. Gonzalez-Pedro, C. Sima, G. Marzari, P. P. Boix, S. Gimenez, Q. Shen, T. Dittrich, I. Mora-Sero, *Phys. Chem. Chem. Phys.*, 2013, **15**, 13835-13843.

ToC Text:

Heterovalent element substitution at metal and chalcogen sites of PbS has been achieved during film formation. The dopants introduced free carriers in the semiconductor affecting the Fermi energy, which has been located by scanning tunneling spectroscopy (STS) studies that have correspondence to density of states (DOS) of a semiconductor.

ToC Graphics: